Optical label-free and model-free probe of the surface potential of nanoscale and microscopic objects in aqueous solution

Cornelis Lütgebaucks,[1] Grazia Gonella,[2,*] and Sylvie Roke[1,*]

[1]*Laboratory for fundamental BioPhotonics (LBP), Institute of Bioengineering (IBI), and Institute of Materials Science (IMX), School of Engineering (STI), and Lausanne Centre for Ultrafast Science (LACUS), École Polytechnique Fédérale de Lausanne (EPFL), CH-1015 Lausanne, Switzerland*

[2]*Max Planck Institute for Polymer Research, Ackermannweg 10, 55128 Mainz, Germany*

(Received 31 May 2016; revised manuscript received 15 August 2016; published 10 November 2016)

The electrostatic environment of aqueous systems is an essential ingredient for the function of any living system. To understand the electrostatic properties and their molecular foundation in soft, living, and three-dimensional systems, we developed a table-top model-free method to determine the surface potential of nano- and microscopic objects in aqueous solutions. Angle-resolved nonresonant second harmonic (SH) scattering measurements contain enough information to determine the surface potential unambiguously, without making assumptions on the structure of the interfacial region. The scattered SH light that is emitted from both the particle interface and the diffuse double layer can be detected in two different polarization states that have independent scattering patterns. The angular shape and intensity are determined by the surface potential and the second-order surface susceptibility. Calibrating the response with the SH intensity of bulk water, a single, unique surface potential value can be extracted. We demonstrate the method with 80 nm bare oil droplets in water and ∼50 nm dioleoylphosphatidylcholine (DOPC) and dioleoylphosphatidylserine (DOPS) liposomes at various ionic strengths.

DOI: 10.1103/PhysRevB.94.195410

I. INTRODUCTION

The electrostatic potential of interfaces drives diverse processes such as self-assembly [1,2], transport [3,4], chemical reactions [5,6], electrochemical processes [7,8], and many other phenomena in biology and chemistry. The stability of nanoparticles, nanoemulsions, micelles [9,10], and their electrochemical reactivity is influenced by the surface potential. Membrane/liposome fusion is governed by surface potentials as well. What all of these systems and processes have in common is that they are composed of nano- or micron-sized structures in aqueous solution. It is the aim of this work to provide a label-free and interface model-free, optical method to determine the surface potential of such particles in aqueous solution.

The electrostatic surface potential, Φ_0, of an object in solution with a radius R is $\Phi_0 = -\int_{\infty}^{R} E_{\mathrm{dc}}(r)dr$, where r indicates the distance away from the interface and E_{dc} is the total electrostatic field that emerges from all possible sources of charges in solution [11]. Obtaining a (surface) potential from a planar macroscopic electrode is generally a complex task as it typically involves measuring an electric current and/or charge distribution that needs to be attributed to a variety of different sources [12]. For a solution of small particles, such measurements are not possible, and the situation is even more complex. Traditionally, for particle dispersions, one employs electrokinetic mobility measurements [13,14] that result in a ζ potential. This quantity is commonly interpreted as the electrostatic potential at the slipping plane of the diffuse double layer (DDL). The position of this hypothetical plane varies with electrolyte concentration and is typically thought of as being positioned up to a few nanometers away from the actual interfacial plane [13–15]. To estimate a value for the surface potential Φ_0 from the ζ potential, the interfacial structure is represented by a simplified mean field model, such as the (planar) Gouy-Chapman (GC) or the constant capacitor (CC) model [15]. In the GC model, which relates Φ_0 to the surface charge density (σ_0), with the electrolyte concentration as variable parameter, the interface is represented by a uniformly charged surface that is embedded in a continuous dielectric medium. Ions are represented as point charges that screen the electrostatic field from the interface. Hydration, changes in the water structure, and specific surface chemistry are neglected.

Spectroscopic measurements offer a way to access the surface potential more directly. X-ray photoelectron spectroscopy measurements were recently proposed as a way to determine the surface potential of silica nanoparticles in highly concentrated solutions [16], but it is yet unclear how applicable the method is in general, as all measurements to date have been performed at synchrotron facilities that have a superior brilliance over table-top sources. Nonresonant second harmonic scattering (SHS) is an optical process used to probe the net orientational order of water molecules along the surface normal (see Ref. [17] and references therein). It is thus sensitive to the orientational directionality of water molecules in the interfacial region defined as the region from the surface plane to the position where the electrostatic field has decayed to zero [18]. Angle-resolved (AR) nonresonant SHS (AR-SHS) [19] is applicable to a wide variety of hard [20–24] and soft particles systems [25–27] and can be used in very dilute solutions and small sample volumes. In absence of chemical effects, the measured intensity depends quadratically on the surface potential [28]. In practice, one who aims to extract the surface potential from a nonresonant SHS experiment applies the following 'Eisenthal-$\chi^{(3)}$ method' [29]: The SH intensity scattered by particles in solutions is measured at a fixed scattering angle as a function of the ionic strength (c) of the solution in any (unspecified) polarization combination. This now widely applied procedure [20,23,27,29,30] is very similar to the method applied to planar interfaces [31–36] using the same expressions. However, by relying on a single equation

*Corresponding authors: gonella@mpip-mainz.mpg.de; sylvie.roke@epfl.ch

to extract three parameters from an arbitrarily normalized data set, a unique solution for Φ_0 cannot be obtained. In addition, the use of the GC or another interface model involuntary restricts the surface structure to a highly idealized composition, as described above, and throws all molecular level information away, even though they are present in the data [18,37].

In this work, we show that it is possible to obtain a unique solution for the surface potential of nanoscopic and microscopic particles in aqueous solution, without the need to invoke a model for the structure of the interfacial region. In our table-top method, we utilize the entire angular scattering pattern in multiple polarization combinations and describe it with nonlinear light scattering theory. In fact, AR-SHS measurements can be described by exact analytical expressions and the parameters are expressed in absolute units. To do this, it is necessary to calibrate the measured intensity against the nonresonant SH response of water. The surface potential and one nonvanishing surface susceptibility tensor element that describes orientational order of water at the surface are the only two independent parameters. The fit of the experimental data collected in two different polarization combinations results in two unique values because two independent equations with two independent parameters are used. The method is applied to three different systems in aqueous solution: nanoscopic oil droplets, zwitterionic and negatively charged single component liposomes composed of either dioleoylphosphatidylcholine (DOPC) or dioleoylphosphatidylserine (DOPS) as a function of the solution's ionic strength. We first describe the SHS experiment and expressions followed by the implementation and application to the three different systems.

II. RESULTS AND DISCUSSION

A. The AR-SHS

In an AR-SHS experiment, a laser beam interacts with an aqueous solution that contains small droplets, particles, or liposomes [Fig. 1(a); see Methods in the Supplemental Material [38] and Ref. [39] for details]. The SHS photons with half the wavelength of the fundamental beam are created in locations where the liquid molecules in the dispersion are not isotropically distributed. These noncentrosymmetric regions are located at the interfacial region of the particle, which consists of the electrical double layer region (i.e., the interface and the DDL around it). The interface may perturb the overall isotropic distribution of water molecules. This gives rise to scattered SH photons [1 in Fig. 1(b)]. The magnitude of the response is determined by computing the orientational average of the second-order hyperpolarizability tensor ($\boldsymbol{\beta}^{(2)}$) elements of water. This procedure results in values for the surface second-order susceptibility, $\boldsymbol{\chi}_s^{(2)}$, tensor elements of the interfacial water [40,41]. In addition, an electrostatic field that originates from a surface charge distribution may generate a small amount of nonisotropically oriented water molecules that can also act as sources of SH photons [on the surface and in the double layer, 2, 3 in Fig. 1(b)]. Furthermore, isotropically oriented water molecules possess a third-order molecular hyperpolarizability tensor ($\boldsymbol{\beta}^{(3)}$) [42] that can also couple with the incoming optical fields and the electrostatic field to give rise to additional emitted SH photons [4 in Fig. 1(b)]. This last contribution is, however, expected to be

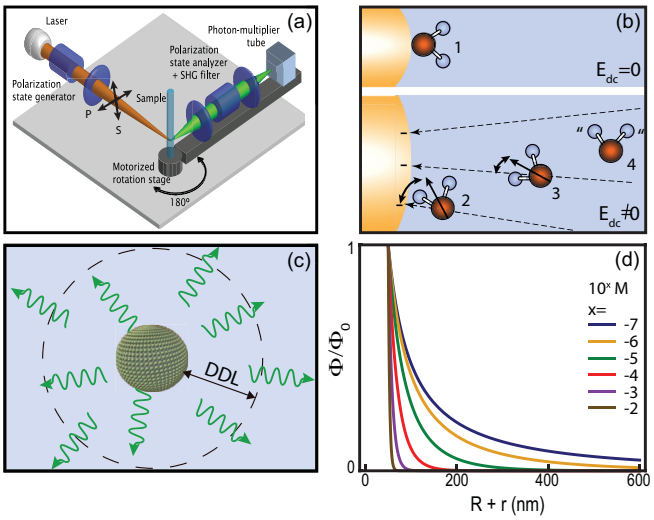

FIG. 1. The SH scattering setup and the nonlinear scattering process from the DDL. (a) The SH scattering setup. The P and S indicate the respective polarization directions as sketched. (b) Molecular sources for possible SH scattering: (1) the breaking of centrosymmetry by an interface ($\boldsymbol{\chi}_s^{(2)}$) or an electrostatic field that reorients the molecules (2) at the surface or (3) in the bulk and (4) the third-order response of isotropic molecules ($\boldsymbol{\beta}^{(3)}$). (c) Illustration of how SHS photons are scattered from the interface and from oriented water molecules in the entire DDL. (d) Illustration of the decay of the surface potential into the solution as a function of the distance away from the center of the sphere ($r + R$), radius $R = 50$ nm.

responsible for less than 1% of the emitted intensity [43]. These four contributions all depend linearly on the electrostatic field and contribute to an effective third-order susceptibility tensor, $\boldsymbol{\chi}^{(3)'}$ [28]. The orientationally correlated, nonisotropic water molecules together emit a SH scattering pattern that appears as though it originates from various dilute hydration shells of very weakly oriented water molecules that surround the droplet or liposome [18,44,45] [Fig. 1(c)]. The interfacial region that contributes to the SH intensity consists of the interface and the entire DDL, that is, up to the distance that the surface potential has decayed to zero. To illustrate this distance and its dependence on the ionic strength and particle radius R, we plot in Fig. 1(d) an exponentially decaying electrostatic potential emanating from a charged spherical nanoparticle with $R = 50$ nm (using $\Phi(r) = \Phi_0 \frac{R}{r} e^{-\kappa(r-R)}$ [12]). Here, κ is the inverse of the Debye length, $\kappa^{-1} = \sqrt{\frac{\varepsilon_0 \varepsilon_r k_B T}{2000\, e^2 z^2 N_A\, c}}$, with $\varepsilon_0, \varepsilon_r, k_B, T$, e, z, N_A, c being the vacuum and relative permittivity, Boltzmann constant, temperature, elementary charge, valency, Avogadro's number, and ionic strength (in mol/L), respectively. The thickness of the weakly oriented hydration layer can be significant and depends on the ionic strength of the solution. This explains the reason that the emitted SH pattern is very sensitive to the structure of the interfacial water, the thickness of the DDL, and the surface potential. These three parameters are represented by the second-order surface susceptibility ($\boldsymbol{\chi}_s^{(2)}$) (at $r = 0$, i.e., at surface of the droplet/liposome), the Debye length (κ^{-1}), and the surface potential (Φ_0), respectively.

As worked out in detail [18,28], the emitted SH intensity $I(2\omega)$ that depends on these three parameters appears in

two independent polarization combinations of the incoming and emitted light, namely in the PPP and PSS polarization combinations [defined in Fig. 1(a), where the first letter refers to the polarization state of the SH beam while the second and third letter refer to that of the fundamental beam]. The polarization- and angle-dependent intensity at a frequency of 2ω is

$$I_{\mathrm{P}ii}(2\omega,\theta) = 2n(2\omega)\sqrt{\varepsilon_0/\mu_0}|E_{\mathrm{P}ii}(2\omega,\theta)|^2, \tag{1}$$

where $n(2\omega)$, ε_0, and μ_0 are the refractive index of the material, permittivity, and permeability of vacuum, respectively, and i is a placeholder for the polarization state of the incoming beams, which can either be S or P.

Using the assumptions detailed in the Supplemental Material [38], we are left with two independent equations for the emitted SH electric field amplitude (one for PPP and one for PSS $\equiv$ SPS $\equiv$ SSP) in two independent unknowns: $\chi^{(2)}_{\mathrm{s},2}$ and Φ_0. We obtain then a unique solution that allows for the determination of the surface potential Φ_0 without making any assumptions about the structure of the DDL or interface in terms of the structure, density, or distribution of charges such as one commonly finds in models describing the electric double layer [13,14].

B. The AR-SHS theory

The amplitude of the two independent scattered SH field components of $\boldsymbol{E}(2\omega)$, $E_{\mathrm{PPP}}(2\omega)$, and $E_{\mathrm{PSS}}(2\omega)$ are

$$\begin{aligned} E_{\mathrm{PPP}}(2\omega) &= \frac{ick_0^2}{2\pi|\hat{r}||\hat{I}|}\frac{e^{ik_0r_0}}{r_0}E_P(\omega)^2\Bigg[\cos\left(\frac{\theta}{2}\right)^3\Gamma_1^{(2)} \\ &\quad + \cos\left(\frac{\theta}{2}\right)\left(\Gamma_2^{(2)}+\Gamma_2^{(3)'}\right)(2\cos(\theta)+1)\Bigg] \\ E_{\mathrm{PSS}}(2\omega) &= \frac{ick_0^2}{2\pi|\hat{r}||\hat{I}|}\frac{e^{ik_0r_0}}{r_0}E_S(\omega)^2\cos\left(\frac{\theta}{2}\right)\left(\Gamma_2^{(2)}+\Gamma_2^{(3)'}\right). \end{aligned} \tag{2}$$

The product $|\hat{r}||\hat{I}|$ is a unit vector product of a distance and current and is needed to preserve the SI units. In the equation, c is the speed of light, θ is the scattering angle [illustrated in Fig. 1(a)], and $\Gamma_1^{(2)}$,$\Gamma_2^{(2)}$ and $\Gamma_2^{(3)'}$ are nonzero elements of the effective particle second- and third-order susceptibility [18,37,46]. These quantities capture the combined symmetry of the scatterers and the incoming electromagnetic fields, the interfacial structure and the electrostatic field in the aqueous phase [46]. The total effective particle susceptibility is a function of the surface second-order susceptibility ($\chi_{\mathrm{s}}^{(2)}$) and the effective third-order susceptibility ($\chi^{(3)'}$) elements [which have the three sources illustrated in Fig. 1(b)], the radius of the particle (R), and the magnitude of the scattering wave vector ($q = |\mathbf{q}| = |\frac{4\pi\, n_{\mathrm{H_2O}}}{\lambda_{\mathrm{SH}}}\sin\frac{\theta}{2}|$). The four independent elements of the effective particle susceptibility for spheres are

$$\begin{aligned} \Gamma_1^{(2)} &= (2F_1(qR) - 5F_2(qR))\,\chi_{\mathrm{s},1}^{(2)''}, \\ \Gamma_2^{(2)} &= F_2(qR)\chi_{\mathrm{s},1}^{(2)''} + 2F_1(qR)\chi_{\mathrm{s},2}^{(2)''}, \\ \Gamma_1^{(3)'} &= 0, \\ \Gamma_2^{(3)'} &= 2\,\chi_2^{(3)''}\Phi_0(F_1(qR) + F_3(qR,\kappa R)), \end{aligned} \tag{3}$$

where $\chi_{\mathrm{s},1}^{(2)''}$ and $\chi_2^{(3)''}$ are second- and third-order susceptibilities that are corrected for changes in the refractive index following Ref. [47]. The expressions are given in Table SI of the Supplemental Material [38]. $F_{1,2,3}$ are analytical goniometric scattering form factors that depend on R, q, and in the case of F_3, also on κ. All these parameters are known. Thus, the quantities in Eq. (3) can be calculated. The analytical expressions for the nonzero tensor elements of the surface susceptibility ($\chi_{\mathrm{s},1}^{(2)''}$, $\chi_{\mathrm{s},2}^{(2)''}$), the DDL ($\chi_2^{(3)''}$), the form factor functions ($F_{1,2,3}$), and the scattering vector ($\mathbf{q}$) are given in Table SII in the Supplemental Material [38].

C. Implementation

In order to obtain reliable and reproducible SHS values independent of the used setup and alignment, we normalize the AR-SHS intensity as follows:

$$S_{\mathrm{P}ii}(\theta) = \frac{I_{\mathrm{P}ii}(\theta) - I_{S,\mathrm{P}ii}(\theta)}{I_{W,\mathrm{SSS}}(\theta)}. \tag{4}$$

We subtract the incoherent SH intensity scattered from the solution without droplets/liposomes, $I_{S,\mathrm{P}ii}(\theta)$ (hyper-Rayleigh scattering), from that of the sample, $I_{\mathrm{P}ii}(\theta)$, measured in the same polarization combination. The result is divided by the hyper-Rayleigh scattering intensity of bulk water in the SSS polarization combination, $I_{W,\mathrm{SSS}}(\theta)$. The i indicates the polarization direction, S or P, of the incoming beams. This normalization also provides an absolute scale to compare different systems.

Since we are working in the dilute regime, multiple scattering events can safely be disregarded. The intensity from the particles in the focal volume will be given by the intensity scattered by a single particle multiplied for the number of particles in this volume. The AR-SHS data in the two independent polarization combinations, normalized by the bulk water signal, can then be expressed using the result from Ref. [18] as a starting point as follows:

$$\begin{aligned} \frac{I_{\mathrm{PPP}}(\theta)}{I_{\mathrm{SSS}}(\theta)} &= \frac{\left(E_P(\omega)^2\left[\cos\left(\frac{\theta}{2}\right)^3\Gamma_1^{(2)} + \cos\left(\frac{\theta}{2}\right)\left(\Gamma_2^{(2)}+\Gamma_2^{(3)'}\right)(2\cos(\theta)+1)\right]\right)^2}{\bar{\mu}^2 N_b/N_p} \\ \frac{I_{\mathrm{PSS}}(\theta)}{I_{\mathrm{SSS}}(\theta)} &= \frac{\left(E_S(\omega)^2\left[\cos\left(\frac{\theta}{2}\right)\left(\Gamma_2^{(2)}+\Gamma_2^{(3)'}\right)\right]\right)^2}{\bar{\mu}^2 N_b/N_p}, \end{aligned} \tag{5}$$

where $\bar{\mu} = \bar{\beta}^{(2)}_{\mathrm{H_2O}}E(\omega)^2$, N_p is the density of droplets/liposomes, and N_b is the density of bulk water (3.34×10^{28} molecules/m^{-3}). N_b/N_p represents the number of bulk water molecules per droplet/liposome. Using Eqs. (5) to describe data processed according to Eq. (4), the values of $\chi^{(2)}_{\mathrm{s},2}$ and Φ_0 are obtained independently.

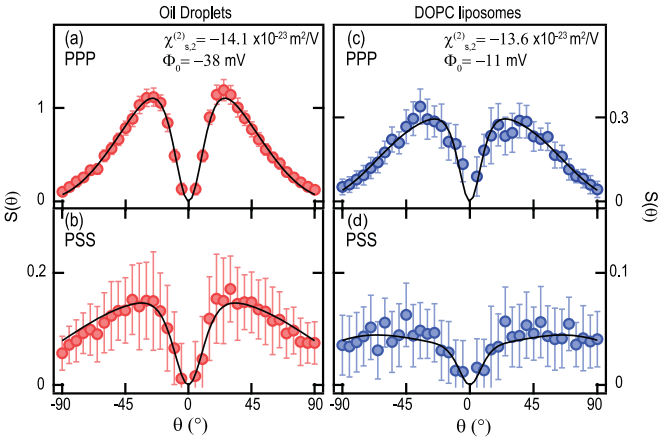

FIG. 2. Scattering patterns of hexadecane droplets [red, panels (a) and (b)] and DOPC liposomes [blue, panels (c) and (d)] in water. The polarization combinations PPP (PSS) are shown on the top (bottom). Error bars represent the standard deviation from 20 measurements.

D. Oil droplets and DOPC liposomes in aqueous solutions

Figures 2(a) and 2(b) show SHS scattering patterns obtained for a solution of hexadecane droplets ($R = 80$ nm) in a weakly basic solution. This system is chosen (and is different from surfactant stabilized droplets studied in Refs. [18,45,48]) as the magnitude and origin of the surface charges on neutral droplets or air bubbles continues to be a matter of debate [49]. Having a reliable value of the surface potential will remove uncertainty as to what the magnitude and sign of the surface potential is, which is still not understood [50]. The error bars represent the standard deviation from 20 measurements. The scattering patterns are different for the PPP and PSS polarization combinations. The black lines are fits to Eqs. (5); the experimental parameters are given in Table SI in the Supplemental Material [38]. As discussed in a previous paper [18], AR-SHS patterns of droplets at very low ionic strength present a very peculiar shape induced by the $F_3(qR,\kappa R)$ factor. Thanks to the normalization by the bulk water signal described by Eq. (4) and the use of Eq. (5), it is now possible to fit the data (black lines) and independently determine $\chi^{(2)}_{s,2} = -(1.41 \pm 0.20) \times 10^{-22}$ m^2/V and $\Phi_0 = -(38 \pm 15)$ mV for the droplet system. The given error in the potential takes into account the variations from the experimentally determined parameters (the radius, the number density, and $\chi^{(2)}_{s,2}$). The corresponding value of the ζ potential is $\zeta = -(32 \pm 9)$ mV, which is similar in magnitude. Here, the error represents the standard deviation of the measured distribution.

DOPC is a zwitterionic phospholipid. DOPC liposomes are therefore expected to have a negligible surface potential. The data in Figs. 2(c) and 2(d) show scattering patterns of DOPC liposomes ($R = 47$ nm) in water. The fit to Eq. (5) (black lines) is obtained for $\chi^{(2)}_{s,2} = -(1.36 \pm 0.20) \times 10^{-22}$ m^2/V and $\Phi_0 = -(11 \pm 10)$ mV. The value of the ζ potential obtained for this system is $\zeta = -(6 \pm 7)$ mV. Both values indeed indicate that the DOPC interface has negligible or a very small electrostatic surface potential.

E. The $\chi^{(2)}_s$

The values of $\chi^{(2)}_{s,2}$ obtained for oil droplets and DOPC liposomes, respectively, $-(1.41 \pm 0.20) \times 10^{-22}$ m^2/V and $-(1.36 \pm 0.20) \times 10^{-22}$ m^2/V, are comparable in magnitude and sign. The $\chi^{(2)}_{s,2}$ is a measure of the orientation of the water molecules at the interface. Our observation thus supports the idea that an electrostatic field, such as that present in the Stern layer, is not strong enough to affect the shape of the orientational distribution function of water molecules [51]. These values are also in good agreement with the nonresonant value of $\chi^{(2)}_{s,2,\text{eff}} = -(1.30 \pm 0.40) \times 10^{-22}$ m^2/V obtained from sum-frequency generation experiments [52], performed on the air/liquid interface. They are also within the range of $\chi^{(2)}_{s,2}$ values of -0.04×10^{-22}m^2/V and -2.26×10^{-22} m^2/V found from numerical simulations [53,54].

F. The DOPS liposomes in aqueous solutions vs ionic strength

The DOPS liposomes were prepared in solutions with different amounts of NaCl. Figures 3(a) and 3(b) show SHS patterns obtained in PPP and PSS polarization combinations with varying ionic strength. The SHS intensity decreases when the ionic strength is increased, and further addition of salt up to 100 mM (not shown) does not induce further changes in the AR-SHS patterns. The decrease is expected as the surface charges are effectively reduced and the size of the DDL is decreased [Fig. 1(d)]. This, in turn, reduces not only the extent of the somewhat ordered water molecules contributing to the scattered SH light but also the effective radius of the probed soft shell [Fig. 1(c)], which further diminishes the scattered SH intensity. The data was fit with a single value of $\chi^{(2)}_{s,2} = -(1.40 \pm 0.20) \times 10^{-22}$ m^2/V, since the values of the electrostatic potential in this range are insufficient to alter the orientational distribution of water [18,51]. From the global fit, using the experimental parameters of Table SIII in the Supplemental Material [38], the values obtained for Φ_0 range from -149 ± 30 mV for 0.15 mM ionic strength down to -23 ± 30 mV at 10 mM and are plotted in Fig. 3(c). The predicted trend is in agreement with expectations: The surface potential is found to decrease with the ionic strength. The ζ potential varies between $-52\,\text{mV} < \zeta < -34\,\text{mV}$ for all solutions, in agreement with earlier measurements [55–57]. The fact that overall $|\zeta| < |\Phi_0|$ is reasonable since ζ is measured at the slipping plane, which is located at some distance away from the interface, and it does not represent the surface potential [13].

G. Comparison between the extracted values and GC or CC solutions

Finally, we examine how our Φ_0 values for DOPS compare to the spherical GC or spherical CC models [58]. To do this we compute solutions for the surface potential as a function of ionic strength for a given surface charge density, which relates to the degree of ionization of the lipids in the outer leaflet [11]. The dashed blue lines in Fig. 3(c) correspond to solutions to the spherical GC model (Eq. 7.11.11 in Ref. [12]), with a surface charge density that corresponds to 80%, 20%, 10%, 8%, 5%, and 3% ionization of PS head groups in the outer leaflets of

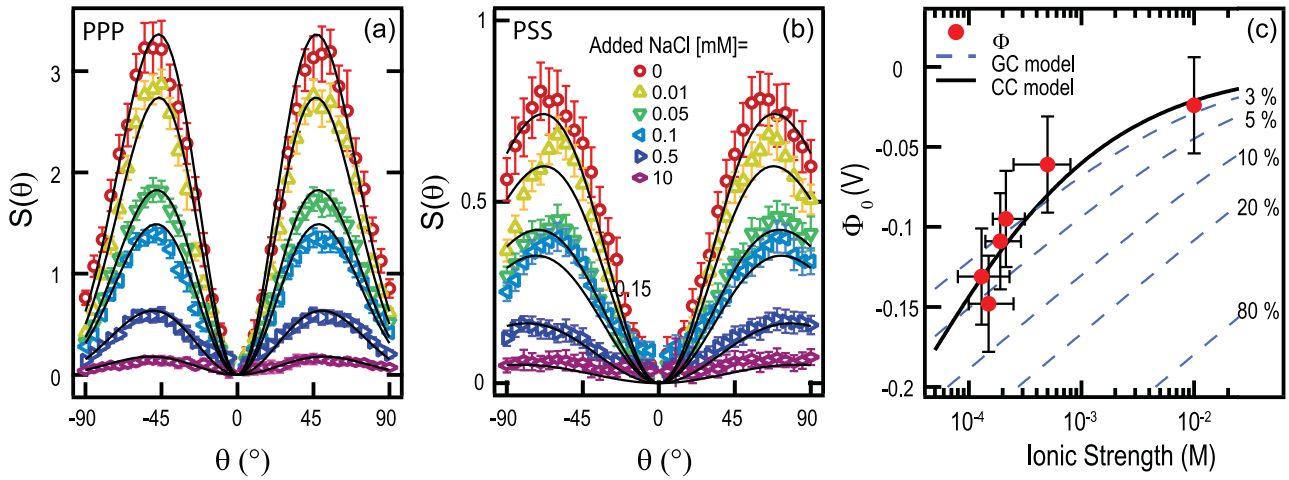

FIG. 3. The SHS patterns from DOPS liposomes in solution. (a) The PPP and (b) PSS polarization combination. Error bars represent the standard deviation of 20 measurements. (c) The extracted surface potential vs ionic strength. Error bars consider the standard deviations for $\chi^{(2)}_{s,2}$, the number density, and the radius. The dashed blue lines represent surface potential values calculated with the GC model for spherical particles [61] using different surface charge densities σ_0 (indicated as degree of ionization of the DOPS head groups in the outer leaflet). The solid black line represents a fit using the spherical CC model. Table SI in the Supplemental Material (see Ref. [38]) contains all experimental parameters to compute the plotted values.

the membrane of DOPS liposomes, assuming a head group area of 0.653 nm^2 [59]. It can be seen that a single GC curve cannot fully capture all the data. Within the assumption that the interfacial water can be treated as a bulk dielectric and that ions are point charges without hydration shells, this suggests that the charge density of the interface may change with ionic strength. Hence the phospholipid dissociation decreases with increasing ionic strength. The solid black line represents a solution to the spherical CC model, assuming a lipid head group ionization of $\sim 2\%$ ($\sigma_0 = (-5 \pm 0.6) \times 10^{-3}\,C/m^2$) (Eq. 50 in Ref. [58]). Within this model, a constant degree of lipid ionization describes the observed trend with a similar accuracy as the GC model except for the DOPS liposomes in pure water. Although we have no information about the validity of the assumptions in both models, a comparison to the data suggests that the degree of ionization of the liposomes is below 20% of all available charges in the outer leaflet of the membrane. Interestingly, Riske *et al.* determined the ionization of dimyristoylphosphatidylglycerol (DMPG) liposomes in pure water based on linear light scattering techniques and a modified GC model considering the association constants of ions [60]. They found an ionization of 12%, which is comparable to what we report.

III. CONCLUSIONS

In the present paper, we demonstrate that by employing nonresonant AR-SHS measurements that are calibrated by the incoherent response of bulk water, unique values for the surface potential of nanoscopic objects in aqueous solutions can be obtained. The method has been successfully applied to aqueous dispersions of nanoscopic oil droplets ($\Phi_0 = -38$ mV), DOPC ($\Phi_0 = -11$ mV), and DOPS liposomes at different ionic strengths ($-148\,\text{mV} < \Phi_0 < -23$ mV) and enables the analysis of potentials in charge neutral and low ionic strength dispersions. Since the values are derived from analytical expressions, without assuming a certain simplified model for the distribution of ions in the electrical double layer, the hydration structure of ions, and the orientation of water molecules, they are extremely useful for theoretical work. In addition, as this experimental table-top method is noninvasive and applicable to aqueous solutions with particles that have sizes up to several microns [62], it will be of great value to characterize and understand the electrostatic properties and molecular structure of many biologically and chemically relevant interfaces.

ACKNOWLEDGMENTS

This paper is supported by the Julia Jacobi Foundation and the European Research Council (Grants No. 240556 and No. 616305). G.G. acknowledges the Donors of the American Chemical Society Petroleum Research Fund for partial support in the initial stages of this research (Grant No. 52618-ND6). We thank Nikolay Smolentsev for the preparation and measurement of the oil nanodroplets.

C.L. and G.G. contributed equally to this work.

[1] V. Liljestrom, J. Seitsonen, and M. A. Kostiainen, ACS Nano **9**, 11278 (2015).

[2] X. Y. Sun, D. H. Bamford, and M. M. Poranen, J. Virol. **88**, 7112 (2014).

[3] H. F. Lodish, *Molecular Cell Biology* (W.H. Freeman, New York, 2000).

[4] R. L. McCreery, Beilstein J. Nanotechnol. **7**, 32 (2016).

[5] Y. Zhang and P. S. Cremer, Annu. Rev. Phys. Chem. **61**, 63 (2010).

[6] M. D. Baer, A. C. Stern, Y. Levin, D. J. Tobias, and C. J. Mundy, J. Phys. Chem. Lett. **3**, 1565 (2012).

[7] C. D. Taylor, S. A. Wasileski, J. S. Filhol, and M. Neurock, Phys. Rev. B **73**, 165402 (2006).

[8] C. T. Konek, M. J. Musorrafiti, H. A. Al-Abadleh, P. A. Bertin, S. T. Nguyen, and F. M. Geiger, J. Am. Chem. Soc. **126**, 11754 (2004).

[9] R. Shah, D. Eldridge, E. Palombo, and I. Harding, *Lipid Nanoparticles: Production, Characterization and Stability* (Springer International Publishing, Swinburne, Australia, 2015).

[10] S. McLaughlin, Annu. Rev. Biophys. Biophys. Chem. **18**, 113 (1989).

[11] D. J. Griffiths, *Introduction to Electrodynamics* (Prentice Hall, Upper Saddle River, N.J., 1999).

[12] R. J. Hunter, *Foundations of Colloid Science* (Oxford University Press, Sydney, 2002).

[13] R. J. Hunter, *Zeta Potential in Colloid Science* (Academic Press, Sydney, 1981).

[14] J. Lyklema, *Fundamentals of Interface and Colloid Science: Liquid-Fluid Interfaces* (Academic Press, Wageningen, Netherlands, 2000).

[15] H. Oshima, *Theory of Colloid and Interfacial Phenomena* (Academic Press, Tokyo, Japan, 2006).

[16] M. A. Brown, Z. Abbas, A. Kleibert, R. G. Green, A. Goel, S. May, and T. M. Squires, Phys. Rev. X **6**, 011007 (2016).

[17] S. Roke and G. Gonella, Annu. Rev. Phys. Chem. **63**, 353 (2012).

[18] G. Gonella, C. Lütgebaucks, A. G. F. de Beer, and S. Roke, J. Phys. Chem. C **120**, 9165 (2016).

[19] B. Schürer, S. Wunderlich, C. Sauerbeck, U. Peschel, and W. Peukert, Phys. Rev. B **82**, 241404(R) (2010).

[20] R. K. Campen, A. K. Pymer, S. Nihonyanagi, and E. Borguet, J. Phys. Chem. C **114**, 18465 (2010).

[21] G. Gonella and H. L. Dai, Langmuir **30**, 2588 (2014).

[22] B. Schürer and W. Peukert, Part. Sci. Technol. **28**, 458 (2010).

[23] R. R. Kumal, T. E. Karam, and L. H. Haber, J. Phys. Chem. C **119**, 16200 (2015).

[24] B. Schürer, M. Hoffmann, S. Wunderlich, L. Harnau, U. Peschel, M. Ballauff, and W. Peukert, J. Phys. Chem. C **115**, 18302 (2011).

[25] R. Scheu, Y. Chen, H. B. de Aguiar, B. M. Rankin, D. Ben-Amotz, and S. Roke, J. Am. Chem. Soc. **136**, 2040 (2014).

[26] N. Smolentsev, C. Lütgebaucks, H. I. Okur, A. De Beer, and S. Roke, J. Am. Chem. Soc. **138**, 4053 (2016).

[27] Y. Liu, E. C. Y. Yan, X. Zhao, and K. B. Eisenthal, Langmuir **17**, 2063 (2001).

[28] A. G. F. de Beer, R. K. Campen, and S. Roke, Phys. Rev. B **82**, 235431 (2010).

[29] E. C. Y. Yan, Y. Liu, and K. B. Eisenthal, J. Phys. Chem. B **102**, 6331 (1998).

[30] C. Sauerbeck, B. Braunschweig, and W. Peukert, J. Phys. Chem. C **118**, 10033 (2014).

[31] S. Ong, X. Zhao, and K. B. Eisenthal, Chem. Phys. Lett. **191**, 327 (1992).

[32] F. M. Geiger, Annu. Rev. Phys. Chem. **60**, 61 (2009).

[33] X. Zhao, S. Ong, and K. B. Eisenthal, Chem. Phys. Lett. **202**, 513 (1993).

[34] X. Zhao, S. Ong, H. Wang, and K. B. Eisenthal, Chem. Phys. Lett. **214**, 203 (1993).

[35] J. N. Malin and F. M. Geiger, J. Phys. Chem. A **114**, 1797 (2010).

[36] C. S. Tian, N. Ji, G. A. Waychunas, and Y. R. Shen, J. Am. Chem. Soc. **130**, 13033 (2008).

[37] A. G. F. de Beer and S. Roke, J. Chem. Phys. **132**, 234702 (2010).

[38] See Supplemental Material at http://link.aps.org/supplemental/10.1103/PhysRevB.94.195410 for details about the chemicals, sample preparation, and characterization; the measurement methods (Table S1); the SH equations that were used for the computations (Table S2); and the assumptions to derive the fitting algorithm (Table S3).

[39] N. Gomopoulos, C. Lütgebaucks, Q. Sun, C. Macias-Romero, and S. Roke, Opt. Express **21**, 815 (2013).

[40] X. Zhuang, P. B. Miranda, D. Kim, and Y. R. Shen, Phys. Rev. B **59**, 12632 (1999).

[41] H. F. Wang, W. Gan, R. Lu, Y. Rao, and B. H. Wu, Int. Rev. Phys. Chem. **24**, 191 (2005).

[42] R. W. Boyd and B. R. Masters, *Nonlinear Optics* (Academic Press, Rochester, 2008).

[43] Y. Chen, H. I. Okur, N. Gomopoulos, C. Macias-Romero, P. S. Cremer, P. B. Petersen, G. Tocci, D. M. Wilkins, C. Liang, M. Ceriotti, and S. Roke, Sci. Adv. **2**, e1501891 (2016).

[44] Note that since isotropically oriented water molecules do not contribute to the signal, tiny fluctuations in the water structure are sufficient to generate enough SH photons.

[45] Y. X. Chen, K. C. Jena, C. Lutgebaucks, H. I. Okur, and S. Roke, Nano. Lett. **15**, 5558 (2015).

[46] S. Roke, M. Bonn, and A. V. Petukhov, Phys. Rev. B **70**, 115106 (2004).

[47] J. I. Dadap, J. Shan, K. B. Eisenthal, and T. F. Heinz, Phys. Rev. Lett. **83**, 4045 (1999).

[48] Y. X. Chen, K. C. Jena, and S. Roke, J. Phys. Chem. C **119**, 17725 (2015).

[49] J.-S. Samson, R. Scheu, N. Smolentsev, S. W. Rick, and S. Roke, Chem. Phys. Lett. **615**, 124 (2014).

[50] N. Agmon, H. J. Bakker, R. K. Campen, R. H. Henchman, P. Pohl, S. Roke, M. Thämer, and A. Hassanali, Chem. Rev. **116**, 7642 (2016).

[51] A. G. F. de Beer and S. Roke, J. Chem. Phys. **145**, 044705 (2016).

[52] S. Yamaguchi, K. Shiratori, A. Morita, and T. Tahara, J. Chem. Phys. **134**, 184705 (2011).

[53] K. Shiratori, S. Yamaguchi, T. Tahara, and A. Morita, J. Chem. Phys. **138**, 159901 (2013).

[54] V. P. Sokhan and D. J. Tildesley, Mol. Phys. **92**, 625 (1997).

[55] F. C. Tsui, S. A. Sundberg, and W. L. Hubbell, Biophys. J. **57**, 85 (1990).

[56] D. J. Crommelin, J. Pharm. Sci. **73**, 1559 (1984).

[57] A. Christiansson, L. E. G. Eriksson, J. Westman, R. Demel, and A. Wieslander, J. Biol. Chem. **260**, 3984 (1985).

[58] P. C. Hiemenz and R. Rajagopalan, *Principles of Colloid and Surface Chemistry* (Marcel Dekker, New York, 1997).

[59] H. I. Petrache, S. Tristram-Nagle, K. Gawrisch, D. Harries, V. A. Parsegian, and J. F. Nagle, Biophys. J. **86**, 1574 (2004).

[60] K. A. Riske, M. J. Politi, W. F. Reed, and M. T. LamyFreund, Chem. Phys. Lipids **89**, 31 (1997).

[61] S. H. Behrens and D. G. Grier, J. Chem. Phys. **115**, 6716 (2001).

[62] A. G. F. de Beer and S. Roke, Phys. Rev. B **79**, 155420 (2009).